University of
Strathclyde
Glasgow

Cruickshank, I. and Gurney, William and Veitch, A.R. (1999) The characteristics of epidemics and invasions with thresholds. Theoretical Population Biology, 56 (3). pp. 279-292. ISSN 0040-5809 ,

This version is available at https://strathprints.strath.ac.uk/41807/

TPB

The Characteristics of Epidemics and Invasions with Thresholds

Isla Cruickshank, William S. C. Gurney,[1] and A. Roy Veitch

Department of Statistics and Modelling Science, University of Strathclyde, Glasgow G1 1XH,
Scotland, United Kingdom

In this paper we report the development of a highly efficient numerical method for determining the principal characteristics (velocity, leading edge width, and peak height) of spatial invasions or epidemics described by deterministic one-dimensiohal reaction–diffusion models whose dynamics include a threshold or Allee effect. We prove that this methodology produces the correct results for single-component models which are generalizations of the Fisher model, and then demonstrate by numerical experimentation that analogous methods work for a wide class of epidemic and invasion models including the S–I and S–E–I epidemic models and the Rosenzweig–McArthur predator–prey model. As examplary application of this approach we consider the atto–fox effect in the classic reaction–diffusion model of rabies in the European fox population and show that the appropriate threshold for this model is within an order of magnitude of the peak disease incidence and thus has potentially significant effects on epidemic properties. We then make a careful re-parameterisation of the model and show that the velocities calculated with realistic thresholds differ surprisingly little from those calculated from threshold-free models. We conclude that an appropriately thresholded reaction–diffusion model provides a robust representation of the initial epidemic wave and thus provides a sound basis on which to begin a properly mechanistic modelling enterprise aimed at understanding the long-term persistence of the disease. © 1999 Academic Press

1. INTRODUCTION

The spatial spread of newly introduced species or diseases is a subject of continuing interest to both theoreticians and empiricists. One strand of theoretical developments (e.g., Skellam, 1951; Kendall, 1965; Mollison, 1972; Murray, 1989) built on the pioneering work of Fisher (1937), who used a logistic-based reaction–diffusion model to investigate the spread of an advantageous gene in a spatially extended population. With initial conditions corresponding to a spatially localised introduction, such models predict the eventual establishment of a well-defined invasion front which divides the invaded and uninvaded regions and moves into the uninvaded region with constant velocity.

Provided that very small populations grow in the same way as finite ones, the velocity at which an invasion front moves is set by the rate of divergence from the (unstable) invader-free state, and can thus be determined by linear methods (e.g., Murray, 1989). These techniques have been refined by Thieme (1979), van den Bosch *et al.* (1990), and Kot *et al.* (1996), who used a closely related renewal equation formalism to facilitate the inclusion of latent periods and more general and realistic transport models. All the analytic work and most of the simulations reported in these papers depend on the assumption that the invaders do not exhibit any special dynamics at very low densities. Where this assumption is not justified, for example when there is an Allee effect (Allee, 1931) the wave speed is determined by the flux of individuals into the region of negative growth ahead of the main front. Although numerical work (e.g., Kot *et al.*, 1996) has

---

[1] To whom correspondence should be addressed.

shown that such effects always slow down the front relative to the threshold-free case, analytic treatment of this intrinsically non-linear class of problems has proved elusive, the only counter-example being Lewis and Kareiva's (1993) treatment of a one-component system with cubic growth dynamics.

Despite their popularity, deterministic representations of the spatial dynamics of invasions and epidemics which assume that finite and infinitesimal populations have indistinguishable dynamics, suffer from a generic difficulty first identified by Mollison (1972, 1991). Far behind the invasion or epidemic front, most epidemic models settle to a spatially homogeneous equilibrium state in which all the players co-exist at finite abundances. In many cases, however, the passage from the epidemic front to co-existence passes through conditions where the local abundances of some or all of the players drops to truly microscopic levels. Worse, local rekindling of the disease usually takes place not because of the immigration of infectives but by *in situ* infections produced by the non-biological remnants of previous populations. Mollison (1991) refers to this, not inconsiderable, infelicity as "the atto-fox problem."

A related difficulty is observed in spatial predator–prey models. Sherrat *et al.* (1995, 1997) have made careful observations of the behaviour of a variety of deterministic predator–prey models in the wake of invasion fronts. Where the local dynamics are strongly damped, the system passes uncontroversially to spatially homogeneous co-existence. However, where the local dynamics are weakly damped or locally unstable, they observe persistent complex wakers which are frequently chaotic. They note that such wakes invariably contain local regions in which the abundance of one or more of the players falls to microscopic levels and that recovery from these events involves *in situ* (and thus unbiological) regrowth rather than immigration from more highly populated regions.

Gurney and Nisbet (1998) show that preventing unbiological infections stemming from microscopic remanent populations in the SEI epidemic model has a relatively minor effect on the propagation of the initial epidemic front but causes a dramatic change in the wake following that front. The complex wake caused by unbiological re-infection is replaced by simple extinction of disease and recovery of the susceptible population to carrying capacity. A parallel investigation of the Rosenzweig–McArthur predator–prey model (Gurney *et al.*, 1998) produced very similar conclusions. This leads us to conclude that the complex chaotic wakes observed by Sherrat *et al.* (1997) depend on *in situ* regrowth. When this is prevented they are replaced by simple prey depletion, leading to predator extinction and eventual prey recovery to carrying capacity.

Gurney *et al.* (1998) show that this change in post-invasion behaviour has very significant consequences for long-term population persistence. In essence, the initial invasion (or epidemic) front is followed by a region of prey (or susceptible) depletion which the predators (or infectives) cannot cross. Long-term persistence of the predator or disease thus requires either very long range dispersal of viable groups of individuals or the formation of spatially ordered structures such as spiral waves. Gurney *et al.* (1998) develop a series of low threshold approximations for the principal characteristics of the invasions predicted by the Rosenzweig–McArthur model and show that these are adequate predictors of the properties of one- and two-dimensional soliton and spiral-wave solutions obtained by direct simulation.

Although the characteristics which facilitate the development of these low threshold approximations are common in predator–prey systems, they are seldom found in realistic epidemic models. Although *in situ* regrowth can often be prevented by the ad hoc choice of a very small threshold, the biologically appropriate threshold value for many epidemic systems is large enough to cause a significant change in propagation velocity.

In this paper, we address the problem of determining those characteristics of epidemics and invasions which are robustly predicted by deterministic models with thresholds. Our first target was the velocity of propagation of the main epidemic front. Although we have been unable to improve on the linear zero-threshold result as an analytic predictor, we have been able to develop an extremely efficient numerical method with essentially arbitrary accuracy. For one-species models we can prove the correctness of this method. The extension to multi-component systems such as the SEI model is essentially heuristic, but a considerable quantity of numerical cross-checking has failed to unearth a single instance where its results are inconsistent with full simulations taking three to four orders of magnitude longer to perform. We have also been able to extend the method to provide values for the spatial extent of the initial invasion front and the peak density of predators (or infectives) contained in it.

Our paper concludes by extending the model of European fox rabies developed by Anderson *et al.* (1981) and Murray (1989) to include a threshold effect. We chose this system as an exemplary application of the methodology developed in this paper because its parameters are well known, and because the likely threshold is a substantial proportion of the peak incidence—leading us to expect a significant reduction in

epidemic velocity. However, because the transmission coefficient is estimated by observing that the epidemic dies out at a given (low) carrying capacity, the parameter revisions which accompany the introduction of a threshold return our velocity estimate to a value close to the zero-threshold result. Thus, the only effect of adding a realistic threshold to the fox-rabies epidemic model is to eliminate the erroneous behaviour in the wake of the primary epidemic wave—that is, the atto-fox effect.

## 2. ONE-COMPONENT SYSTEMS

2.1. General Treatment

In this section we consider a generalisation of the model introduced by Fisher (1937) to describe the invasive spread of a diffusively dispersing organism with logistic local dynamics. If we represent the density of the organism at time T and position X by $N(X, T)$, then the model is

$$\frac{\partial N}{\partial T} = QN\left(1 - \frac{N}{K}\right) + \Psi \frac{\partial^2 N}{\partial X^2}, \tag{1}$$

where Q is the intrinsic growth rate, K is the carrying capacity, and Ψ is the diffusion coefficient. We recognise the inverse of the intrinsic growth rate Q^{-1}, the carrying capacity K, and the diffusion length $\sqrt{\Psi/Q}$ as the natural scales of time, population, and length, respectively. We define scaled population, time, and distance as $n \equiv N/K$, $t \equiv QT$, and $x \equiv X\sqrt{Q/\Psi}$, respectively. Thus, without any loss of generality, we restate the model as

$$\frac{\partial n}{\partial t} = n(1 - n) + \frac{\partial^2 n}{\partial x^2}. \tag{2}$$

The properties of this model are well known (Skellam, 1951; Hadeler and Rothe, 1975; Murray, 1989). If a propagule of individuals is introduced into a previously empty system, the local population grows towards the carrying capacity and spreads into the surrounding empty territory. Eventually, the invaded and uninvaded regions are separated by a narrow "invasion front," which moves into the uninvaded territory at constant speed. Although the front velocity formally depends on the initial condition, all initial conditions with compact support excite a front traveling at the minimum possible scaled velocity, which can be shown to be $v = 2$. This is equivalent to an unscaled velocity $V = 2\sqrt{Q\Psi}$.
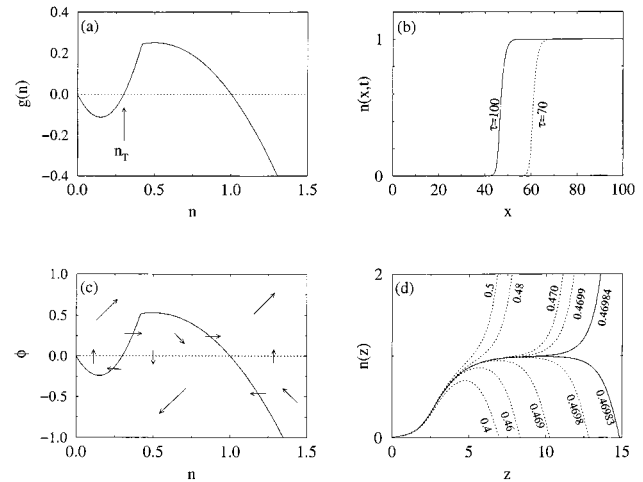
FIG. 1. Generic behaviour of the model defined by Eq. (3)—specific $g(n)$ given by Eq. (11) with $a = 1.5$ and $n_T = 0.3$. (a) Net growth function. (b) Typical invasion front. (c) Phase-plane analysis with $v_R = 0.47$: solid line shows the isocline implied by Inequality (8). (d) Group of solutions for $z > 0$ in a moving frame of reference (Eq. (5))—each labelled with the valve of v_R.

To generalise this model, we define $g(n)$ to represent the (scaled) local net population growth rate, and so write

$$\frac{\partial n}{\partial t} = g(n) + \frac{\partial^2 n}{\partial x^2}. \tag{3}$$

For the Fisher model, $g(n) = n(1 - n)$, implying positive growth for any population between zero and the carrying capacity ($n = 1$). We want to represent a situation where very small populations cannot grow, so we assume that $g(n)$ has the form typified by Fig. 1a: negative for n below a threshold value n_T, positive for $n_T < n < 1$, negative for $n > 1$, and zero at n equals 0, n_T, and 1.

We want to study an invasion front moving from right to left as shown in Fig. 1b. We therefore transform the problem into a frame of reference moving leftwards at speed v_R, by defining new variables $z \equiv x + v_R t$ and $\phi(z) \equiv dn/dz$. For a front travelling with constant shape, n depends only on z, so we can re-express Eq. (3) as

$$\frac{dn}{dz} = \phi, \qquad \frac{d\phi}{dz} = v_R \phi - g(n). \tag{4}$$

If we place the zero of z at a point where $n = n_0 \ll n_T < 1$ then Eq. (4) can be approximated for $z \leqslant 0$ by

$$\frac{d^2 n}{dz^2} - v_R \frac{dn}{dz} + g'(0)\, n = 0 \quad \text{where} \quad g'(0) \equiv \left[\frac{dg}{dn}\right]_{n=0} < 0. \tag{5}$$

This has two solutions of the form $n = n_0 e^{\lambda z}$. Any solution with $\lambda > 0$ goes to zero as $z \to -\infty$ and is thus of the form which we require. Hence we can deduce that

$$\lambda = \tfrac{1}{2}(v_R + \sqrt{v_R^2 - 4g'(0)}). \tag{6}$$

Hence, for $z \geqslant 0$ we solve Eq. (4) subject to the initial conditions

$$n(0) = n_0, \qquad \phi(0) = \lambda n_0. \tag{7}$$

We can deduce the characteristics of the resulting solutions from a phase-plane analysis. Inspection of Eq. (4) shows that the condition for n to increase with z is just $\phi > 0$, while the condition for ϕ to increase with z is

$$\phi > \frac{g(n)}{v_R}. \tag{8}$$

The implications of these conditions, and especially the boundary between the regions in which ϕ increases and decreases, are illustrated in Fig. 1c.

We first consider solutions with a given value of v_R, $n(0) = n_0 \ll n_T < 1$, and *arbitrary* (positive) values of $\phi(0) = \phi_0$. For large enough values of v_R, all such trajectories tend to $n = \infty$ as $z \to \infty$. At lower values of v_R there are three possibilities. For a single value of ϕ_0, which we denote by $\phi_c(v_R)$, the trajectory hits the steady state $(1, 0)$. For $\phi_0 > \phi_c(v_R)$, $n \to \infty$ as $z \to \infty$, while for $\phi_0 < \phi_c(v_R)$, the trajectory rises to a value above $n = n_T$ and below 1 before eventually falling back below $n = n_T$. In Appendix A we show that ϕ_c is a non-increasing function of v_R.

We now consider solutions with the initial value of ϕ linked to the frame of reference velocity v_R by setting $\phi_0 = \lambda n_0$ with λ given by Eq. (6). We shall restrict ourselves to growth functions which permit the formation of an invasion front. Thus, if we set v_R to the exact value of the front velocity v, the trajectory must be that which hits $(1,0)$, and we know that $\lambda(v) n_0 = \phi_c(v)$. If we now consider a trajectory generated with $v_R < v$ then we know from Eq. (6) that $\phi_0 = \lambda(v_R) n_0 < \lambda(v) n_0$. But, since ϕ_c is a non-increasing function of v_R, we know that $\phi_c(v_R) \geqslant \phi_c(v) = \lambda(v) n_0$. Hence we can be sure that $\phi_0 < \phi_c(v_R)$ and thus that the trajectory falls into the class which rise to a value between n_T and unity before eventually falling back below zero. An essentially parallel argument shows that if we set $v_R > v$ the solution always tends monotonically to $n = \infty$ as $z \to \infty$.

As we illustrate in Fig. 1d, the behaviour implied by this argument appears highly inconvenient, because it requires us to set the frame of reference velocity exactly

equal to the front velocity if we wish our solution to represent the wave-front correctly. However, viewed from a different perspective it provides us with a way of determining whether the frame of reference velocity is greater than or less than the (unique) front velocity, and thus of determining the front velocity by a simple bisection search.

2.2. The Fisher Equation with an Allee Effect

As an example of the class of systems discussed above, we extend the basic Fisher model to include an Allee effect (Allee, 1937). Specifically, we imagine an organism with a linearly density dependent per capita death rate, D, and a per capita fecundity rate, B, which is constant (B_0) at high densities, but increases linearly with slope B_1 at low densities. That is, we write

$$D = D_0 + D_1 N \quad B = \begin{cases} B_0 & N > (B_0/B_1) \\ B_1 N & \text{otherwise.} \end{cases} \tag{9}$$

If we define $Q \equiv B_0 - D_0$ and $K \equiv Q/D_1$ then these assumptions imply that the unscaled net growth function $G(N)$ is

$$G(N) = \begin{cases} QN(1 - N/K) & N > (B_0/B_1) \\ -D_0 N + (B_1 - D_1) N^2 & \text{otherwise.} \end{cases} \tag{10}$$

Adopting the scaling which led to Eq. (2), and defining $a \equiv D_0/(B_0 - D_0)$ and $n_T \equiv a D_1/(B_1 - D_1)$ we find that the scaled equivalent of this expression is

$$g(n) = \begin{cases} n(1 - n) & n > n_s \\ a(n/n_T)(n - n_T) & \text{otherwise} \end{cases} \tag{11}$$

where

$$n_s \equiv \frac{1 + a}{1 + (a/n_T)}. \tag{12}$$

In this parameterisation, n_T represents the scaled threshold value and $-a$ is the slope of the growth function at $n = 0$. To determine the initial condition for Eq. (4) we set $n_0 = \min(0.001, n_T/100)$, use Eq. (6) to relate λ to our choice of v_R, and thus determine $n(0)$ and $\phi(0)$ from Eq. (7). We then conduct a bisection search, starting with $v_R = -1$ and $v_R = 2$, which we know must bracket the actual velocity. The centre point of the interval is tested by solving Eq. (4) and determining if the solution passes above unity or falls back below threshold. In the first case the test velocity is above the front velocity
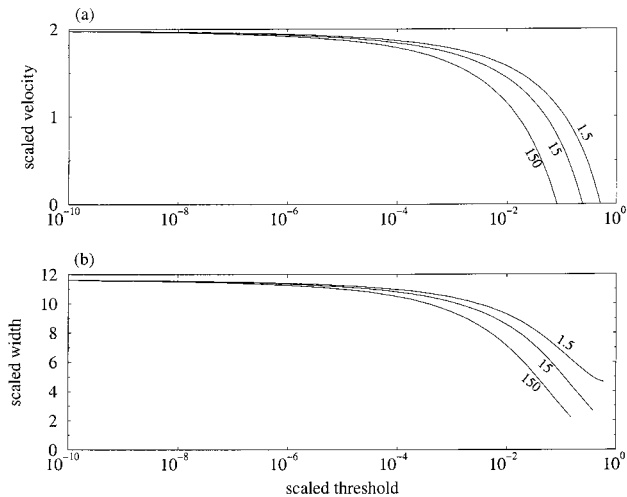
FIG. 2. Scaled front velocity (a) and width (b) as a function of scaled threshold (n_T), for the model defined by Eq. (4) and (11). Values of a marked on each curve. Velocities determined by a 20 step bisection search starting on $[-1, 2]$. Widths determined to 1 in 10^3.

and the centre point becomes the high end of the new bracketing pair. In the second, it is below and the centre point becomes the low end of the next bracket. Twenty repetitions of this procedure, which takes about 0.1 s on a medium power workstation, gives the scaled front velocity to 1 in 10^6.

In Fig. 2a we show the relation between scaled front velocity and threshold for three values of a. In all cases the velocity converges slowly to the non-threshold system value, $v = 2$, as $n_T \to 0$. As we would expect, finite thresholds slow up the front. At $n_T \approx 10^{-4}$ the velocity is reduced by about 10%, while at $n_T \approx 10^{-2}$ the velocity is reduced by between 20% and 40%. As the threshold approaches unity, forward propagation stops at a critical threshold which depends strongly on a. For thresholds in excess of the critical value, the dynamic equations formally possess a solution of the same form but with a negative velocity. However, with any biologically realistic initial invasion, this solution corresponds to the extinction of the invading propagule.

A further possibility is suggested by Fig. 1d which shows the behaviour of this system for $a = 1.5$, $n_T = 0.3$. As v_R converges towards the exact front velocity v, the solution of Eq. (4) follows the exact wave shape for longer and longer before diverging off to zero or ∞. Thus, by running the bisection process for more iterations than are needed to measure the front velocity, we can use the same calculation to give us an estimate of the front width, which we define as the distance between the points at which $n(z) = 0.05$ and 0.95. The values shown in Fig. 2b were determined by a calculation which terminated whenever the estimates of this quantity from the

current upper and lower bracket velocities differed by less that 1 part in 10^3. In practice this normally requires between 5 and 50 extra iterations, so the computational cost, although much increased over that of simple velocity determination, remains trivial.

We see from Fig. 2b that the scaled width of the invasion front changes quite markedly with its velocity. As the front slows down, it becomes steadily narrower—an effect we would expect if local growth to carrying capacity took a (scaled) time which was essentially constant.

3. TWO-COMPONENT SYSTEMS

We now turn our attention to systems with two players. Since these systems are not as amenable to analysis as their single species counterparts, we examine specific examples.

3.1. The S–I Model

Our first example is a spatial extension of the well-known "susceptible–infective" (S–I) epidemic model. We assume that susceptibles are immobile, and that in the absence of infection their population density, $S(X, T)$, would grow logistically. The conventional version of this model assumes that the per capita rate at which susceptibles become infected is proportional to the local density of infectives, $I(X, T)$, with the constant of proportionality (B) being known as the transmission coefficient. It then assumes that infected individuals suffer per capita mortality at rate D_0 and disperse diffusively with diffusion constant Ψ. Hence the dynamics of the system are

$$\frac{\partial S}{\partial T} = QS\left(1 - \frac{S}{K}\right) - BSI \qquad \frac{\partial I}{\partial T} = (BS - D_0)I + \Psi \frac{\partial^2 I}{\partial X^2}.$$
(13)

The usual interpretation of deterministic models of this kind is that they describe the dynamics of average densities calculated over a (very) large ensemble of replicate systems. Practical biological experiments generally encompass only a modest degree of replication, so we shall take an alternative view in which Eq. (13) are seen as describing averages calculated over a finite-sized ensemble containing N_R replicates.

At time T, each replicate will contain a number of infective and susceptible individuals distributed over the available space. To estimate the ensemble average infective density at X, $I(X, T)$, we define a quadrat of area A_Q

centred at X in each system, count the number of infective individuals contained in this set of quadrats, and divide the result by the product of the quadrat area and the number of replicates. The minimum non-zero value of $I(X)$ occurs when quadrat X contains zero individuals in every replicate except one, where it contains a single individual—a configuration which implies that $I = (N_R A_Q)^{-1}$.

It is thus clear that all values of I in the range $[0, (N_R A_Q)^{-1})$ should be interpreted as representing a condition in which the infective population of quadrat X is extinct. In discrete space/time models which use continuous state variables it is common practice to recognise this by setting local population densities below an appropriate threshold value to zero. However, in a formally continuous space/time model this option is profoundly unappealing since it induces discontinuities in the spatial distribution.

We choose instead to eliminate unbiological behaviour which might result from effectively extinct local populations of infectives by preventing such local populations from producing infections. The most obvious way of doing this would be to set the transmission coefficient (B) to zero for infective populations below a threshold $I_T \approx (N_R A_Q)^{-1}$.

We performed a number of our early experiments using this formulation. Although it turns out to be quite straightforward to generalise the bisection method for numerical velocity determination to tolerate a discontinuous dependence of B on I, it is less easy to perform accurate simulations on this basis. Since the main purpose of this paper is to demonstrate the reliability of the bisection method by detailed comparison with explicit simulations, we chose to implement the threshold effect by assuming a continuous dependence of B on I of the form used in the last section, namely

$$B = \begin{cases} B_0 & I \geqslant I_T B_0 K / D_0 \\ (D_0/K)(I/I_T) & \text{otherwise.} \end{cases} \quad (14)$$

Here, I_T represents the infective density below which the infective population cannot increase, even when the susceptible population is at carrying capacity.

Defining scaled variables $s \equiv S/K$, $i \equiv I/K$, $t \equiv QT$, $x \equiv X\sqrt{Q/\Psi}$ and parameter groups $b_0 \equiv B_0 K/Q$, $d_0 \equiv D_0/Q$, $i_T \equiv I_T/K$ allows us, without losses of generality, to re-express this model as

$$\frac{\partial s}{\partial t} = s(1-s) - bsi \quad \frac{\partial i}{\partial t} = (bs - d_0)\,i + \frac{\partial^2 i}{\partial x^2}, \quad (15)$$

where

$$b = \begin{cases} b_0 & i \geqslant b_0 i_T / d_0 \\ d_0 i / i_T & \text{otherwise.} \end{cases} \quad (16)$$

This model has three, non-trivial, spatially homogeneous stationary states: one with no infectives and susceptibles at carrying capacity, one with high s^* and low i^*, and one with low s^* and high i^*. Provided $i_T < (d_0/b_0^2)(1 - d_0/b_0)$, the high i^* steady state is identical to that of the equivalent un-thresholded model, namely

$$s^* = \frac{d_0}{b_0}, \qquad i^* = \frac{b_0 - d_0}{b_0^2}. \quad (17)$$

So long as this steady state is positive ($b_0 > d_0$) it is locally stable. Spatially uniform perturbations return to it monotonically if

$$b_0 - d_0 < \frac{d_0}{b_0} \quad (18)$$

and return via damped oscillations otherwise.

The properties of the non-threshold version of this model have been investigated by Dunbar (1983, 1984), whose work is summarised in a more approachable form by Murray (1989). For all biologically sensible parameters, introduction of a propagule of infected individuals into a universe previously occupied by susceptibles eventually produces a stable-shaped epidemic front moving at a (scaled) velocity v_0 given by

$$v_0 = 2\sqrt{b_0 - d_0}. \quad (19)$$

When Inequality (18) is fulfilled, the front has at most one overshoot before settling to the steady state given by Eq. (17). Otherwise, the front trails a "wake" of damped oscillations.

When the local dynamics are non-oscillatory or the scaled threshold i_T is small, the behaviour of our modified model is unchanged except for a reduction in front velocity (Fig. 3a). However, the combination of oscillatory dynamics and a finite threshold can produce a radical change in behaviour. In Fig. 3c, the threshold is above the minimum infective density which would occur in the trough behind the initial epidemic if there were no threshold. Now, the infective population does not recover from this trough, but instead declines asymptotically to zero, allowing the susceptible population to recover to the carrying capacity. Thus, in addition to changing the velocity of the front, in this case the
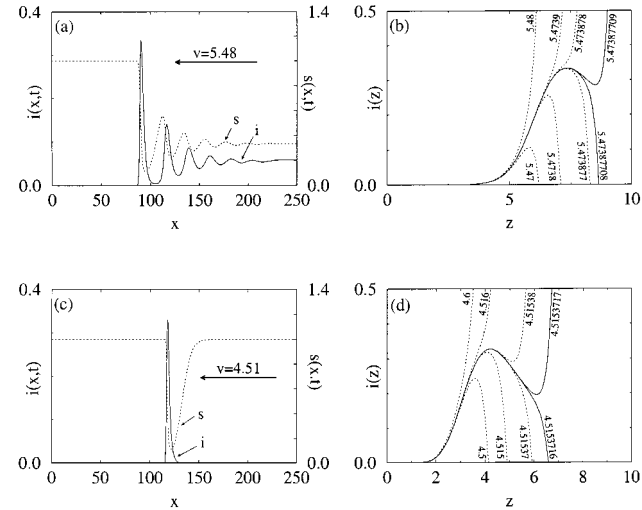
FIG. 3. Epidemic waves in the S–I model with $b_0 = 12$, $d_0 = 4$. Frames (a) and (c) show snapshots of the wavefront at $t = 25$ for $i_T = 10^{-6}$ and 5×10^{-3}, respectively. Frames (b) and (d) show equivalent solutions in frames of reference moving at different (marked) velocities. To obtain (b) and (d) we solved Eqs. (20) and (21) with $s(0) = 1$, $i_0 = i_T \times 10^{-3}$, using RK4 with an allowed error of 1 in 10^6. To obtain (a) and (c) p.d.e.'s (15) were discretised by the method of lines onto a grid with $\Delta x = 0.25$ and the resulting system of o.d.e.'s integrated using RK4 with an allowed error of 1 in 10^4.

threshold has changed the post-epidemic state of the system from a persistent admixture of susceptibles and infectives to one containing only susceptibles.

Guided by the results of the last section we study the behaviour of this system in a frame of reference moving at velocity $-v_R$. Since we are looking for a constant-shape solution, we assume that i and s depend only on $z \equiv x + v_R t$, define $\phi(z) \equiv di(z)/dz$, and hence re-express Eq. (15) as

$$\frac{d\phi}{dz} = v_R \phi - (bs - d_0) i, \qquad \frac{di}{dz} = \phi, \qquad (20)$$

$$\frac{ds}{dz} = v_R^{-1}[s(1 - s) - bsi], \qquad (21)$$

where b is defined by Eq. (16). If we place the zero of z at a point to the left of the front, where $i = i_0 \ll i_T$, then we can be sure that for all $z < 0$, $s(z) \approx 1$ and hence $i(z) = i_0 e^{\lambda z}$, where

$$\lambda = \tfrac{1}{2}[v_R + \sqrt{v_R^2 + 4d_0}]. \qquad (22)$$

Hence, for $z > 0$ we must solve Eq. (20) and (21) subject to the initial conditions $s(0) = 1$, $i(0) = i_0$, and $\phi(0) = \lambda i_0$.

The solutions thus produced, which we illustrate in Figs. 3b and 3d, are strongly reminiscent of those we

obtained for the Fisher equation in the last section. In particular, they follow the true shape of the wavefront for a distance which depends on how close the frame of reference velocity is to a single value, which we hypothesize must be the front velocity in a static frame of reference. If the frame of reference velocity is less than the front velocity then the density of infectives eventually becomes negative, while if $v_R > v$ the infective density diverges to $+\infty$. Although in this case we cannot prove this behaviour to be generic, we have performed a wide-ranging numerical investigation without uncovering a single counterexample.

This regularity of behaviour again presents us with an opportunity to make an efficient numerical determination of the velocity of the epidemic front using a bisection search. In Fig. 4a we show curves of front velocity against threshold infective density calculated in this way. Since we cannot prove that this procedure converges to the correct front velocity, we have also performed direct simulations of the model defined by Eqs. (15) and (16) and measured the asymptotic properties of the epidemic front. We show that the velocities thus observed are in excellent agreement with those predicted by the bisection method. We also notice that as the threshold goes to zero, the bisection method velocity predictions converge
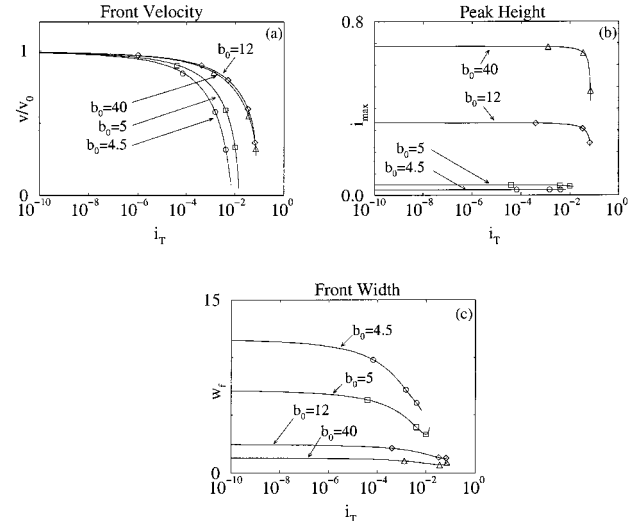
FIG. 4. Properties of epidemic fronts in the S–I model with $d_0 = 4$ and b_0 as marked, plotted against normalised threshold i_T. Smooth curves show results from Eqs. (20) and (21) using the bisection method. Points show results from numerical solution of Eq. (15): $b_0 = 4.5$ (circles), $b_0 = 5$ (squares), $b_0 = 12$ (diamonds), $b_0 = 40$ (triangles). (a) Front velocity, shown as v/v_0 where the zero threshold value $v_0 = 2\sqrt{b_0 - d_0}$. (b) $i_{max} = $ maximum abundance of infectives. (c) $w_f = $ distance between the point where i first exceeds $0.05i_{max}$ and the point where it first exceeds $0.95i_{max}$.

(albeit slowly) to the zero-threshold velocity (v_0) given by Eq. (19).

Figs. 3b and 3d show a further similarity with our earlier findings on the Fisher model, namely that the solutions in a frame of reference moving at velocity v_R follow the correct front shape for a longer and longer distance as v_R approaches the front velocity v. Deducing the whole wave shape from such a calculation would require us to identify the front velocity to an accuracy well beyond the numerical precision of any practicable computing machinery. However, it is entirely possible to make our identification accurate enough to measure the maximum abundance of infectives (i_{max}) and the width of the period of epidemic onset (w_f). In Figs. 4b and 4c we show the values of these quantities inferred from the bisection method calculations, compared with the results of a small number of confirmatory simulations. Again, we see excellent agreement.

3.2. The Rosenzweig–McArthur Model

Our second two-component example is a spatial extension of the Rosenzweig–McArthur predator–prey model (Rosenzweig, 1971). Here we assume that the prey ($F(X, T)$) is immobile and grows logistically with intrinsic growth rate R to a carrying capacity K in the absence of predation. The predators ($C(X, T)$) disperse diffusively with diffusion constant Ψ and suffer density-independent mortality at per capita rate D_0. They kill prey at a rate U given by a Holling type II functional response with maximum uptake rate U_m and half-saturation prey abundance H,

$$U(F) \equiv \frac{U_m F}{F + H}. \tag{23}$$

Ingested prey are turned into new predator individuals with efficiency E. Hence, the dynamics of the system are described by

$$\frac{\partial F}{\partial T} = QF\left(1 - \frac{F}{K}\right) - UC$$
$$\frac{\partial C}{\partial T} = (EU - D_0)\,C + \Psi\frac{\partial^2 C}{\partial X^2}. \tag{24}$$

Provided that predators never become locally scarce this model can safely be assumed to have a constant value of prey–predator conversion efficiency, E_0. However, if reproduction is sexual, then predators present in very small abundances will be unable to mate and hence turn

ingested prey into new predators. To model this effect, we write

$$E = \begin{cases} E_0 & C \geqslant C_T E_0 U_m / D_0 \\ D_0 C/(U_m C_T) & \text{otherwise.} \end{cases} \tag{25}$$

We identify Q^{-1}, $\sqrt{\Psi/Q}$, H, and $E_0 H$ as the natural scales of time, distance, food, and consumer population, respectively, and re-express the model in terms of dimensionless variables $t \equiv QT$, $x \equiv X\sqrt{Q/\Psi}$, $f \equiv F/H$, $c \equiv C/(E_0 H)$, and parameter groups $k \equiv K/H$, $u_m \equiv U_m/Q$, $c_T \equiv C_T/(E_0 H)$; thus

$$\frac{\partial f}{\partial t} = f\left(1 - \frac{f}{k}\right) - uc \qquad \frac{\partial c}{\partial t} = (eu - d_0)\,c + \frac{\partial^2 c}{\partial x^2}, \tag{26}$$

where

$$u = \frac{u_m f}{1 + f} \tag{27}$$

and

$$e = \begin{cases} 1 & c \geqslant c_T u_m / d_0 \\ d_0 c/(u_m c_T) & \text{otherwise.} \end{cases} \tag{28}$$

This model has many similarities to the S–I epidemic model discussed above. It has spatially homogeneous exterior steady states at $(c^*, f^*) = (0, 0)$ and $(0, k)$. Provided

$$c_T < \frac{d_0}{u_m - d_0}\left(1 - \frac{d_0}{k(u_m - d_0)}\right), \tag{29}$$

it has a spatially homogeneous interior steady state

$$f^* = \frac{d_0}{u_m - d_0}, \qquad c^* = (1 + f^*)\left(1 - \frac{f^*}{k}\right), \tag{30}$$

which is identical to that of the equivalent non-thresholded model. However, in contrast to the S–I model case, the interior steady state is locally unstable against spatially uniform perturbations if

$$k > \frac{u_m + d_0}{u_m - d_0}. \tag{31}$$

Invasions in this system behave in a very similar way to the epidemics shown in Fig. 3. When the local dynamics are stable and either strongly damped or non-oscillatory, the invasion front trails a short wake, leading

eventually to spatially uniform co-existence (cf. Fig. 3a). When the local dynamics show oscillatory instability or weakly damped oscillations, the solution takes the form of a soliton (cf. Fig. 3c).

As before, we study the behaviour of such solutions by transforming the system into a frame of reference moving at velocity $-v_R$. Since we are looking for a constant-shape solution, we assume that c and f depend only on $z \equiv x + v_R t$, define $\phi(z) \equiv dc(z)/dz$, and re-express Eq. (26) as

$$\frac{d\phi}{dz} = v_R \phi - (eu - d_0)\, c, \qquad \frac{dc}{dz} = \phi, \qquad (32)$$

$$\frac{df}{dz} = v_R^{-1}[\, f(1 - f/k) - uc\,], \qquad (33)$$

where u is defined by Eq. (27) and e by Eq. (28). If we place the zero of z at a point to the left of the front, where $c = c_0 \ll c_T$, then we can be sure that for all $z < 0$, $f(z) \approx k$ and hence $c(z) = c_0 e^{\lambda z}$ where

$$\lambda = \tfrac{1}{2}[\, v_R + \sqrt{v_R^2 + 4d_0}\,]. \qquad (34)$$

Hence, for $z > 0$ we must solve Eq. (32) and (33) subject to the initial conditions $f(0) = k$, $c(0) = c_0$, and $\phi(0) = \lambda c_0$.

The behaviour of this transformed system is essentially identical to that of the S–I system illustrated in Figs. 3b and 3d. If the frame of reference velocity v_R is greater than the front velocity (v) then the normalized consumer population ($c(z)$) tends to ∞ as z becomes large. If $v_R < v$ then the normalised consumer population eventually becomes negative. As the frame of reference velocity approaches the true front velocity the solution of the transformed system follows the true solution to progressively larger values of z. Although we cannot prove that this behaviour is generic, we have conducted a wide-ranging numerical investigation without finding any counter-examples.

As in the case of the S–I model, this behaviour provides us with an efficient numerical route to determining the velocity of the front by a bisection search. Extending the bisection process to sufficiently high accuracy allows us to determine the characteristics of the early part of the front—namely the peak consumer density and the spatial width of the initial invasion ahead of the peak consumer density.

In Fig. 5 we plot the results of four such investigations, together with a small number of results measured (at many orders of magnitude more labour) from direct
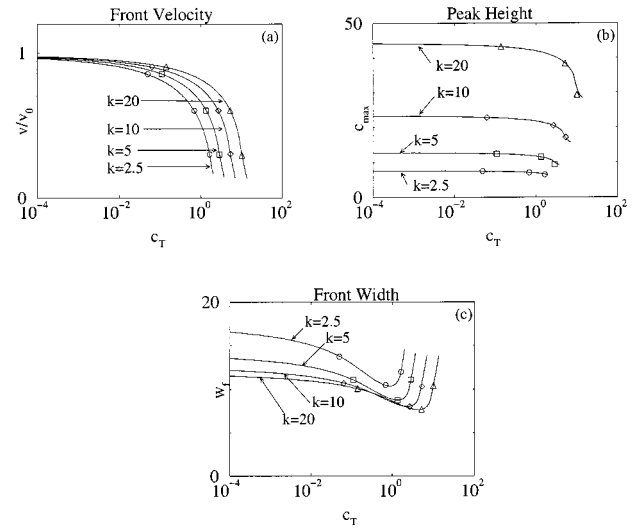
FIG. 5. Properties of epidemic fronts in the Rosenzweig–McArthur model with $u_m = 0.2$, $d_0 = 0.05$, and k as marked, plotted against normalised threshold c_T. Smooth curves: results from Eqs. (32) and (33) using the bisection method. Points: results from numerical solution of Eq. (26): $k = 2.5$ (circles), $k = 5$ (squares), $k = 10$ (diamonds), $k = 20$ (triangles). (a) front velocity, shown as v/v_0 where the zero threshold value $v_0 = \sqrt{u_m - d_0}$. (b) $c_{max} =$ maximum abundance of predators. (c) $w_f =$ distance between the point where c first exceeds $0.05c_{max}$ and the point where it first exceeds $0.95c_{max}$.

solution of the scaled dynamic equations (26). As for the S–I model we see excellent agreement between our bisection method estimates and the confirmatory simulations. In further confirmation, we note that as $c_T \to 0$ the velocity of the invasion front tends (albeit slowly) to the analytic value derived for the threshold-free system.

4. THE S–I MODEL AND EUROPEAN FOX RABIES

Our final example is a spatial variant of the well-known S–E–I epidemic model developed to represent a disease, such as rabies, which has a long incubation period. We consider a one-dimensional universe containing individuals who can be susceptible, exposed (infected) but not infectious, or infectious (rabid). The local susceptible population grows logistically to carrying capacity K. Susceptible individuals are infected by contact with rabid individuals, whereupon they enter the exposed state, from which they have a constant probability per unit time of progressing to the infective stage. This model expresses the dynamics of the normalised populations of susceptibles, exposed and infectives ($S(X, T)$, $E(X, T)$, and $I(X, T)$) as

Parameters for the SIR Fox–Rabies Model

Parameter	Symbol	Value	Units
Carrying capacity	K	$0.2 \rightarrow 4$	km^{-2}
Intrinsic growth rate	Q	0.5	yr^{-1}
Exposed mortality	D_e	0.5	yr^{-1}
Infective (rabid) mortality	D_i	73	yr^{-1}
Transmission coefficient	B	80	km^2/yr
Transfer rate	Θ	13	yr^{-1}
Diffusion coefficient	Ψ	200	km^2/yr

$$\frac{\partial S}{\partial T} = QS\left(1 - \frac{S}{K}\right) - BSI, \qquad \frac{\partial E}{\partial T} = BSI - (D_e + \Theta)\, E \tag{35}$$

$$\frac{\partial I}{\partial T} = \Theta E - D_i I + \Psi \frac{\partial^2 I}{\partial X^2}. \tag{36}$$

The parameters D_e and D_i represent the normalised per capita mortality rates of exposed and infective (rabid) individuals, B is the transmission coefficient, Θ is the transfer rate between exposed and infective categories, and Ψ is the diffusion coefficient. The properties of this model are discussed in Murray (1989) and Gurney and Nisbet (1998), who quote the parameter values reproduced in Table I for rabies in the European fox population.

With these parameters, the model produces invasion fronts which move at velocities comparable to (but arguably somewhat above) those observed in the field. The wake behind the invasion front contains about five after-shocks of diminishing amplitude, and the system eventually settles at the co-existence steady state. Gurney and Nisbet (1998) showed that the occurrence of these after-shocks is critically dependent on re-infection of the susceptible population by unbiologically small remnants of the preceding outbreak. They further showed that if such unbiological remnants were prevented from acting as a source of infection, the invasion front remained relatively unaffected but the wake changed dramatically. The after-shocks disappear entirely, and the eventual state far behind the epidemic is rabies-free, with the susceptibles at their carrying capacity.

To facilitate comparison of bisection method and explicit simulation results, we incorporate a threshold into the model in a slightly less discontinuous way, by assuming that the transmission coefficient is constant (B_0) at high local densities of rabid individuals, but falls linearly with low local densities. We represent this by writing

$$B =$$
$$\begin{cases} B_0 & I \geqslant KB_0 I_T \Theta / (D_i(\Theta + D_e)) \\ [(\Theta + D_e)\, D_i/(\Theta K)](I/I_T) & \text{otherwise,} \end{cases}$$
$$\tag{37}$$

so that the parameter I_T represents the minimum local density of rabid individuals which can grow in the absence of immigration, provided the susceptibles are at carrying capacity.

The relationship between the behaviour of the model defined by Eqs. (35), (36), and (37) and its non-thresholded cousin is very similar to that described by Gurney and Nisbet (1998) and discussed earlier in this paper in the context of the SI model. However, this version of the thresholded SEI model turns out to be susceptible to the treatment described earlier for the SI epidemic model and the Rosenzweig–McArthur predator–prey model. If we transform the system into a frame of reference moving with an arbitrary velocity V_R, then the properties of the resulting solutions depend critically on the relation between V_R and the epidemic front velocity V. If $V_R > V$ then the solution of the transformed system has $I \rightarrow \infty$ as z becomes large, whereas $V < V_R$ implies that I eventually passes below zero. Since the interior steady state is always unstable in the transformed system, all solutions eventually go to ∞ or become negative except in the special case $V_R = V$. As V_R approaches V the solution in the transformed system follows the correct wave shape for an increasing distance in the transformed co-ordinate.

This behaviour implies that the numerical technique explored earlier for finding the properties of epidemic fronts in simpler systems, can also be expected to work here. In Fig. 6 we show the relationship between threshold rabid density (I_T) and front velocity, height, and width for a series of values of carrying capacity spanning the plausible range for the European fox. On the same diagram we show a number of values of the same quantities calculated from direct simulations of Eqs. (35), (36), and (37). Since we see excellent agreement between bisection method results and direct simulations at a widely distributed set of points, we can have confidence that the broad picture shown in this diagram is accurate.

Gurney and Nisbet (1998) showed that with the parameters given in Table I, a threshold as low as $10^{-6}\ km^{-2}$ gives rise to a soliton solution of the type shown in Fig. 3c. Their simulation results suggest that such a low threshold value should affect the epidemic velocity by only a few percent, and this is confirmed by the more accurate calculation leading to Fig. 6. However, this figure also shows that higher values of I_T
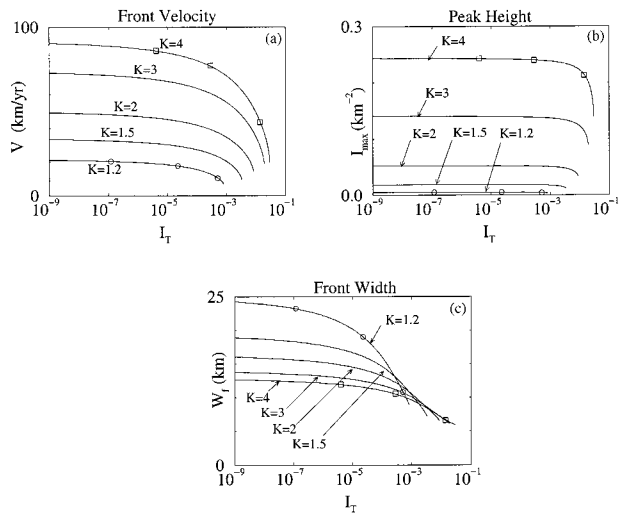
FIG. 6. Properties of epidemic fronts as a function of threshold (I_T) in the thresholded S–I model with parameters from Table I. Curves show values derived from the bisection search method for a given value of K. Points show direct simulation results. (a) Front velocity; (b) peak infective (rabid) density; (c) front width defined as in Fig. 5.

can produce very significant changes in epidemic properties.

To make an estimate of an appropriate threshold in this case, we note that the average lifetime of an individual showing clinical symptoms (and hence acting as a source of infection) is 5 days (0.014 yr). It seems highly unlikely that any infected individual can live for more than twice this period (0.028 yr). Murray (1989) argues that although the diffusion coefficient for rabid foxes is hard to estimate accurately, its value must lie in the range from 70 to 330 km^2 per year. The root mean square displacement of a rabid individual between becoming infective and dying must therefore be between 2.8 and 6.1 km. Since the probability distribution of this displacement is Gaussian, it seems reasonable to assume that any susceptible which does not have at least one rabid individual within three times the root mean square displacement is safe from infection. This implies that I_T lies between 1×10^{-3} km^{-2} and 4.5×10^{-3} km^{-2}.

In terms of our earlier discussion of the interpretation of thresholds, we note that since the peak infective density is on the order of 0.3 km^{-2} (Fig. 6) we should think of the densities in our rabies model as being defined on quadrats with $A_Q \approx 3$ km^2. This implies that with thresholds in the range given above, we should interpret our model as describing the dynamics of averages taken over an ensemble containing between 75 and 330 members.

It is clear from Fig. 6 that a threshold of the order of 2×10^{-3} km^{-2} will decrease the velocity and increase the

width of the epidemic front by around 30 % compared to the values predicted by a model with zero threshold and otherwise identical parameters. However, we recall that the value given in Table I for the transmission coefficient (B_0) was chosen to match the observation that rabies is not self-sustaining when the fox carrying capacity is below a critical value, K_c. Figure 6 implies that at a given value of B_0, the minimum value of K for a self-sustaining epidemic (K_c) depends on I_T. Thus, once a value for I_T has been selected, B_0 must be re-adjusted to return K_c to its observed value, K_c^o.

Observed values of K_c^o cover a range from 0.25 to 1.0 km^{-2} (Lloyd 1976, Andral and Toma 1977). We arbitrarily choose the middle of this range and set $K_c^o = 0.63$ km^{-2}. Since the ratio of the smallest to the largest possible value of diffusion coefficient is nearly 5, we choose as our best estimate of this quantity a value, $\Psi = 150$ km^2 yr^{-1}, which differs from both ends of the range by roughly the same factor (≈ 2.2). In Figs. 7a and 7b we show the best estimate of front velocity and peak rabid abundance calculated using these parameters. Although introducing a threshold with all other parameters held constant always reduces front velocity, the adjustment to B_0 required to return K_c to its observed value K_c^o implies that the results differ little from those derived by Murray (1989) from the zero-threshold version of this model.
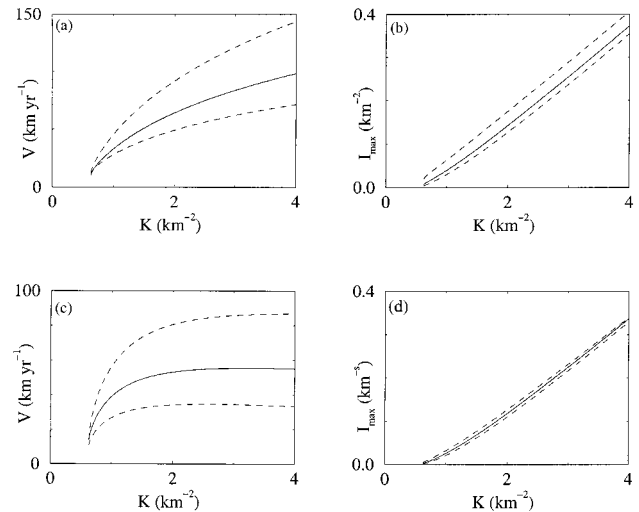
FIG. 7. Predicted characteristics of rabies epidemics in the European fox population. Solid curves show best estimates, dotted curves show values calculated from extremal values of diffusion coefficient. *Upper frames* show velocity (a) and peak incidence (b) with constant diffusion coefficient. $\Psi = 150$ km^2 yr^{-1}, $I_T = 2.1 \times 10^{-3}$ km^{-2}, $B_0 = 221$ km^2 yr^{-1}. *Lower frames* show velocity (c) and peak incidence (d) with $\Psi \propto 1/K$. $\Psi = 300/K$ km^2 yr^{-1}, $I_T = 1.05K \times 10^{-4}$ km^{-2}, $B_0 = 164$ km^2 yr^{-1}.

A characteristic feature of the predictions of both thresholded and non-thresholded SEI models is that the predicted front velocity is a strongly increasing function of carrying capacity. This conflicts with field observations suggesting that the epidemic velocity is always in the range 30–60 km yr^{-1}. In their (linear) treatment, van den Bosch *et al.* (1990) overcome this problem by postulating that the size of fox territories, and hence the diffusion coefficient, is inversely proportional to fox density. To investigate the effect of this assumption in our model, we assume that territory size cannot adjust rapidly to changes in instantaneous density, so that the diffusion constant may be regarded as inversely proportional to carrying capacity K. As a direct corollary of this assumption we also take I_T to be proportional to K. We assume, rather arbitrarily, that our previous evaluation of diffusion constant produced the appropriate result for a fox density of 2 km^{-2}, so we set $\Psi = 300/K$ km^2 yr^{-1} and $I_T = (1.05 \times 10^{-4})\, K$ km^{-2}.

In Figs. 7c and 7d we show the best estimates of front velocity and peak rabid abundance calculated using this prescription and adjusting B_0 so that $K_c = K_c^\circ = 0.63$ km^{-2}. Again, the absolute size of the predicted velocity is surprisingly close to the equivalent zero-threshold results (van den Bosch *et al.* 1990). As we might expect by analogy with that calculation, the key feature of the results from this variant of the model is that over most of the plausible range of carrying capacity, the epidemic velocity is almost independent of K.

The most striking conclusion from both calculations shown in Fig. 7 is that the difference between the velocity predicted by our modified S–E–I model and that predicted by its less biological cousin is dwarfed by the uncertainty in the absolute size of the diffusion coefficient and the dependence (if any) of that diffusion coefficient on carrying capacity. This suggests that those features of the model predictions which are robust against the elimination of unbiological infectivity—mainly the existence and properties of the initial epidemic wave—can safely be modelled by deterministic reaction–diffusion methods with or without thresholds. Those features which are critically dependent on the occurrence of unbiological infection—specifically the passage to a stable endemic—can safely be eliminated from the repertoire of a reaction–diffusion formulation by the addition of a threshold or Allee effect.

5. DISCUSSION

In this paper, we describe an efficient numerical method for determining the characteristics of an epidemic or invasion when the invading organism cannot grow from arbitrarily low densities. This method depends on observing that when we transform the reaction–diffusion description of the system into a moving frame of reference, its properties change dramatically. All the interior steady states become violently unstable and generating a solution which ends on any of them poses a problem akin to firing a ball bearing up a smooth mountainside so that it finishes up balanced on the summit.

The key to exploiting this situation turns out to be the fact that although hitting the steady state requires exact determination of the correct frame of reference velocity and is thus functionally impossible, determining whether the ball passes over the ridge or falls back is simple. Moreover, the distinction between overshooting and falling back turns out to correlate exactly with the relation between the frame of reference velocity and the front velocity—providing a natural route to determining the front velocity to an arbitrary degree of accuracy by a bisection search.

Although we have only proved the correctness of this methodology for the class of single component models formed by generalizing the Fisher model, we have observed experimentally that it works excellently for a wide class of multi-component models including the S–I and S–E–I epidemic models and the Rosenzweig–McArthur predator–prey model, with a variety of alternative representations of low density behaviour.

Although the solution of the transformed system always diverges from the "correct" solution eventually, we observe experimentally that as the frame of reference and front velocities converge, the transformed solution follows the shape of the untransformed solution for progressively longer and longer. This implies that if the bisection process designed to yield velocity estimates is continued to rather higher accuracy than would normally be warranted by epidemic velocity data, the transformed solution follows the untransformed solution far enough for us to be able to reliably determine the characteristics of the leading part of the epidemic wave—specifically the spatial extent of the epidemic onset and the peak incidence of the disease.

The work reported here has shown that the characteristics predicted for the initial epidemic or invasion wave by reaction–diffusion formalisms are qualitatively robust against the elimination of the atto-fox effect (Mollison, 1991). The effect of introducing a preventative threshold or Allee effect is generally to slow up the epidemic front and reduce the peak disease incidence. However, as our application to European fox rabies demonstrated, the particular route by which parameters are estimated can reduce these changes to the point

where they are insignificant compared to the inaccuracies inherent in parameter or structural uncertainty.

Because of the inherent difficulty of estimating diffusion coefficients, explicit inclusion of thresholds or Allee effects seems unlikely to change estimated velocities by observable amounts. However, models incorporating these effects yield robust estimates of the characteristics of the initial epidemic, and are very amenable to efficient numerical estimation of these quantities. In common with their non-thresholded cousins, these models currently have nothing useful to say about the long term persistence of the disease—a problem which clearly requires new observational as well as theoretical insights. However, there are indications that they form a more promising basis for theoretical developments in this area than models which permit unbiological reinfection.

APPENDIX

We seek solutions of

$$\frac{dn}{dz} = \phi \qquad n(0) = n_0, \tag{38}$$

$$\frac{d\phi}{dz} = v_{\mathbf{R}}\phi - g(n) \qquad \phi(0) = \phi_0. \tag{39}$$

This is equivalent to

$$\frac{d\phi}{dn} = \gamma(n, v_{\mathbf{R}}, \phi) \qquad \phi(n_0) = \phi_0, \tag{40}$$

where

$$\gamma(n, v_{\mathbf{R}}, \phi) \equiv v_{\mathbf{R}} - \frac{g(n)}{\phi}. \tag{41}$$

We represent the solution of this system by $\phi(n, v_{\mathbf{R}}, \phi_0)$ and define $\phi_c(v)$ such that $\phi(n, v, \phi_c(v)) \to 0$ as $n \to 1^-$.

We first note that Eq. (41) implies that

$$v_1 > v_2 \Rightarrow \gamma(n, v_1, \phi) > \gamma(n, v_2, \phi), \tag{42}$$

which in turn implies that, so long as $\phi(n, v_1, \phi_0) > 0$,

$$v_1 > v_2 \Rightarrow \phi(n, v_1, \phi_0) \geqslant \phi(n, v_2, \phi_0). \tag{43}$$

Now consider two trajectories, the first calculated with $\phi(n_0) = \phi_c(v_1)$ and $v_{\mathbf{R}} = v_1$, and the second calculated from the same initial condition but with $v_{\mathbf{R}} = v_2 < v_1$. The first trajectory hits $(1, 0)$. Inequality (43) tells us that while the first trajectory is above the *n*-axis, the second trajectory cannot be above it and will generally be below it. The second trajectory thus crosses the *n* axis ($\phi = 0$) at or to the left of $(1, 0)$. If it hits $(1, 0)$ then we know that $\phi_c(v_1) = \phi_c(v_2)$. If it crosses to the left of $(1, 0)$ then the phase plane analysis shown in Fig. 1c implies that to cause it to hit $(1, 0)$ we must use an increased value of $\phi(n_0)$, so $\phi_c(v_1) < \phi_c(v_2)$. Hence, we know that

$$v_1 > v_2 \Rightarrow \phi_c(v_1) \leqslant \phi_c(v_2). \tag{44}$$

ACKNOWLEDGMENTS

REFERENCES

Allee, W. C. 1931. "Animal Aggregations. A Study in General Sociology," Univ. of Chicago Press, Chicago.

Anderson, R. M., Jackson, H. C., May, R. M., and Smith, A. M. 1981. Populations dynamics of fox rabies in Europe, *Nature* **289**, 765–771.

Dunbar, S. R. 1983. Travelling wave solutions of diffusive Lotka–Volterra equations, *J. Math. Biol.* **17**, 11–32.

Dunbar, S. R. 1984. Travelling wave solutions of diffusive Lotka–Volterra equations: A heteroclinic connection in R^4, *Trans. Amer. Math. Soc.* **268**, 557–594.

Fisher, R. A. 1937. The wave of advance of advantageous genes, *Ann. Eugen.* **7**, 353–369.

Gurney, W. S. C., Veith, A. R., Cruickshank, I., and McGeachin, G. 1998. Circles and spirals: Population persistence in a spatially explicit predator–prey model, *Ecology* **79**(7), 2516–2530.

Gurney, W. S. C., and Nisbet, R. M. 1998. *in* "Ecological Dynamics," pp. 308–316, Oxford Univ. Press, New York.

Hadeler, K. P., and Rothe, F., 1975. Travelling wave-fronts in nonlinear diffusion equations, *J. Math. Biol.* **2**, 251–263.

Kendall, D. G. 1965. Mathematical models of the spread of infection, *in* "Mathematics and Computer Science in Biology and Medicine," Medical Research Council, London.

Kot, M., Lewis, M. A., and van den Driessche, P. 1996. Dispersal data and the spread of invading organisms, *Ecology* **77**, 2027–2042.

Lewis, M. A., and Kareiva, P. 1993. Allee dynamics and the spread of invading organisms, *Theor. Popul. Biol.* **43**, 141–158.

Mollison, D. 1972. Possible velocities for a simple epidemic, *Adv. Appl. Probab.* **4**, 233–258.

Mollison, D., 1991. Dependence of epidemic and populations velocities on basic parameters, *Math. Biosci.* **107**, 255–287.

Murray, J. D. 1989. "Mathematical Biology," Springer-Verlag, Heidelberg.

Rosenzweig, M. L. 1971. The paradox of enrichment: The destabilization of exploitation ecosystems in ecological time, *Science* **171**, 385–387.

Sherrat, J. A., Lewis, M. A., and Fowler, A. C. 1995. Ecological chaos in the wake of an invasion, *Proc. Nat. Acad. Sci. U.S.A.* **92**, 2524–2528.

Sherrat, J. A., Egan, B. T., and Lewis, M. A. 1997. Oscillations and chaos behind predator–prey invasion: Mathematical artifact or ecological reality, *Philos. Trans. R. Soc. B*, in press.

Skellam, J. G. 1951. Random dispersion in theoretical populations, *Biometrica* **38**, 196–218.

Thieme, H. R. 1979. Density-dependent regulation of spatially distributed populations and their asymptotic speed of spread, *J. Math. Biol.* **8**, 173–187.

Van den Bosch, F., Metz, J. A. J., and Diekmann, O. 1990. The velocity of spatial population expansion, *J. Math. Biol.* **28**, 529–565.